IEEE Access
Multidisciplinary | Rapid Review | Open Access Journal

Received 17 May 2024, accepted 24 June 2024, date of publication 27 June 2024, date of current version 26 July 2024.

Digital Object Identifier 10.1109/ACCESS.2024.3419844

RESEARCH ARTICLE

Optically Transparent Series-Fed Microstrip Array With Small Inter-Element Spacing and Stepped Feed-Lines for Antenna-on-Display

JIN MYEONG HEO[1], (Graduate Student Member, IEEE), KISEO KIM[2], JAEUK CHOI[2], AND GANGIL BYUN[1], (Senior Member, IEEE)

[1]Department of Electrical Engineering, Ulsan National Institute of Science and Technology (UNIST), Eonyang-eup, Ulju-gun, Ulsan 44919, South Korea
[2]Samsung Display Company Ltd., Kiheung-gu, Yongin 17113, South Korea

Corresponding author: Gangil Byun (byun@unist.ac.kr)

This work was supported by Samsung Display Company Ltd., Kiheung, South Korea.

ABSTRACT This paper proposes an optically transparent series-fed microstrip array with small inter-element spacing and stepped feed lines for antenna-on-display applications. In the proposed series-fed array, the inconsistency of resonant frequencies between the input impedance at the edge of the feed line and the consecutive patch element produces multiple resonant frequencies. The small inter-element spacing in the array reduces input impedance variation among multiple resonant frequencies so that they are closely spaced, forming a broad impedance bandwidth. Also, stepped feed lines allow for impedance matching by a gradual decrease in characteristic impedance. Thus, impedance bandwidth and flat gain of the antenna are enhanced as the number of array elements increases. Optical transparency of the antenna is realized by using thin-metal meshes to be implemented on an active area of display panels. To validate the proposed approach, a 5×1 array antenna is fabricated and measured. The measured results exhibit a -10 dB impedance bandwidth of 14.2% (25.08−28.92 GHz) and 3 dB gain bandwidth of 10.1% (26.2−29 GHz) with 7.02 dBi peak gain at 27.4 GHz. Furthermore, the design is extended to a 5×4 array with a feeding network, demonstrating the beam scanning properties of $\pm 20°$ and $\pm 40°$ at 28 GHz with a bore-sight gain of 11.8 dBi.

INDEX TERMS Series-fed microstrip array, antenna-on-display (AoD), inter-element spacing, stepped feed lines, bandwidth improvement.

I. INTRODUCTION

In recent years, millimeter-wave (mmWave) with broad frequency bandwidth has gained attention for higher data rates in mobile communication [1]. To enable higher data rates, broad impedance bandwidth is required for mmWave antennas as well as high gain to compensate for free-space path loss by a few millimeter-wavelengths [2], [3], [4]. This promotes active research on antenna designs with broadband [5], high gain [6], and beamforming properties by using arrays [7]. However, the space in mobile devices for mmWave antennas is insufficient since the multiple antennas for wireless communications such as universal mobile telecommunication system (UMTS), long-term evolution (LTE), Wi-Fi, and Bluetooth are already equipped in the platforms [8]. Moreover, the remaining space has been reduced due to the preference for narrower bezels [9], [10]. To address this issue, research has been conducted on antenna-on-display (AoD) that places optically transparent antennas on an active area of the display panels. In [11], a transparent conducting oxide (TCO) film is used. The antenna array is made of fluorine-doped tin oxide (FTO) for optical transparency and is positioned below the touch sensor showing an impedance bandwidth of 41%. In [12], the indium tin oxide (ITO) monopole antenna with an optical transparency of 84% and a peak gain of 2 dBi is introduced for smartphone wireless communication purposes. Despite the high transparency, the TCO-based

The associate editor coordinating the review of this manuscript and approving it for publication was Mohammad Tariqul Islam.

antennas suffer from low radiation efficiencies due to the high sheet resistances ($> 4\ \Omega$/sq), which makes them impractical for use in mmWave mobile communications [13]. To attain optical transparency of more than 80% with much lower sheet resistance than TCO-based antennas, thin-metal mesh microstrip antennas are employed in [14], [15], [16], and [17]. In this method, thin-metal lines of the meshes are placed within the micro-scale gap between adjacent light-emitting diodes (LEDs) to ensure both visibility of the display and antenna conductivity. Lee et al. [18] proposed dual-band dual-polarized AoD operating with patch and monopole modes showing a broad bandwidth of 17.8%. Nevertheless, the previous works for AoD applications exhibit gains lower than 4.14 dBi for a single antenna element. Stacked antenna structures [19] and artificial magnetic conductors (AMC) [20] can enhance the impedance bandwidth and gain. However, they are constrained by the manufacturing process because a substantial increase in panel thickness is inevitable. Alternatively, a series-fed microstrip array is suitable for low-profile antenna design [21], [22], [23]. By adopting a large number of array elements, a high antenna gain can be accomplished. Yet, its narrow impedance and gain bandwidths remain challenging issues.

In this paper, we propose an optically transparent series-fed microstrip array with small inter-element spacing and stepped feed lines for AoD. For optical transparency, the patch elements and feed lines are made of rhombus-shaped unit meshes with a metal line width of a few micrometers. We intentionally exploit the inconsistency of resonant frequencies between the input impedance at the edge of the feed line and the consecutive patch element to produce multiple resonant frequencies. By reducing the inter-element spacing, the input impedance variation among the resonant frequencies decreases. This enables the multiple resonant frequencies to be closely spaced, providing a broader impedance bandwidth with higher gain as the number of array elements increases. As a result, the gain bandwidth of the array is also enhanced. To improve impedance matching, the feed line widths are designed in a stepped manner with a gradual decrease in characteristic impedance. For verification, the proposed array antenna composed of thin-metal meshes is fabricated, and its optical transparency, impedance bandwidth, and radiation pattern are measured.

The remainder of this paper is organized as follows: In Section II, the proposed series-fed array design approach is introduced. The input impedance and bandwidth of the proposed array are formulated in this section. Section III presents the simulation studies of design parameters and their efficacy on antenna characteristics. Section IV presents the fabricated optically transparent array antennas with measured results and beamforming properties. Section V concludes the paper.

II. PROPOSED DESIGN APPROACH

Fig. 1(a) illustrates a three-dimensional view of the proposed 5 × 4 array antenna stack up for AoD applications.

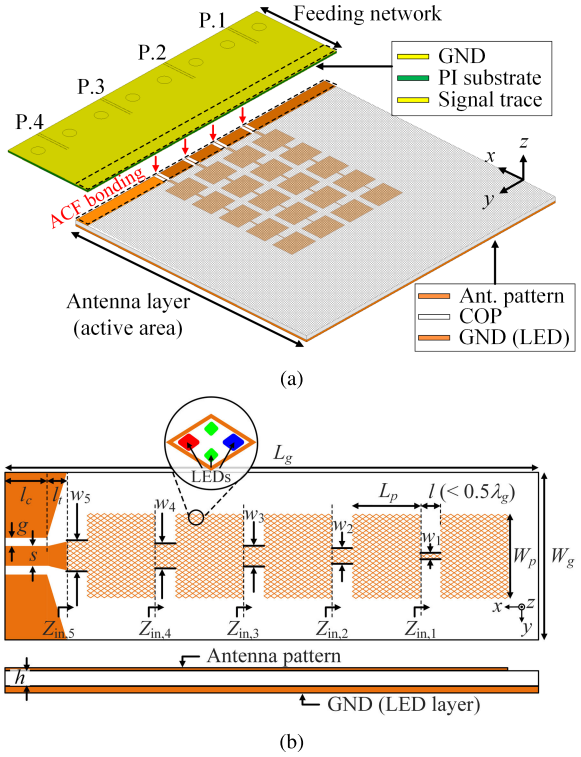

FIGURE 1. Design of the proposed series-fed microstrip array antenna. (a) Three-dimensional view of the 5 × 4 array antenna stack up. (b) Top view and side view of the proposed array with design parameters.

The antenna patterns are printed on a cyclic olefin polymer (COP) film, which is mounted on the active area of the display panel. The feeding network is designed for beamforming and is bent to connect with the backside printed-circuit board (PCB) of the mobile devices. The polyimide (PI) substrate of the feeding network and COP are bonded to each other using adhesive conductive film (ACF). Fig. 1(b) presents a design of the proposed series-fed microstrip array with grounded-coplanar waveguide (GCPW). The overall antenna dimension is $W_g \times L_g = 13$ mm $\times$ 44 mm with a ground (GND) on the bottom and an antenna pattern on the top. The GCPW structure with 50-Ω characteristic impedance is designed for antenna measurements and has a length of $l_c = 5.8$ mm. The signal trace width (s) is 0.3 mm, and the gap between the signal trace and the coplanar GND (g) is 0.13 mm. The GCPW-to-microstrip transition has a length of $l_t = 0.2$ mm with tapered signal trace and coplanar GNDs. For AoD applications, the antenna pattern is made of rhombus-shaped unit meshes that can surround the LEDs in the display panel. The proposed array consists of 5 patches and 5 feed lines printed on a dielectric substrate ($\varepsilon_r = 2.32$, $\tan\delta = 0.0006$) with a height of $h = 0.1$ mm. From right to left, $Z_{\text{in},i}$ ($i = 1, 2, \ldots, 5$) represents the total input impedance at the edge of the feed line connected to the i-th patch element. Note that patch elements in the proposed array have the same dimension of $W_p \times L_p = 4.6$ mm $\times$ 3.58 mm. In this case, the resonant frequency of $Z_{\text{in},i}$ does not coincide with that of the

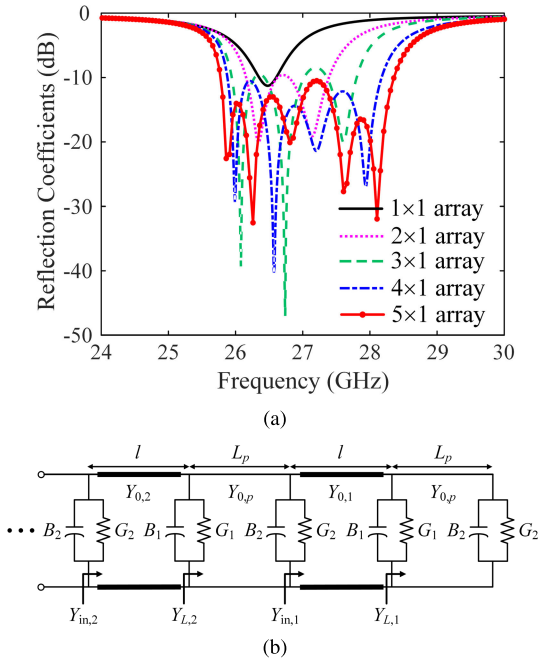

FIGURE 2. (a) Efficacy of the multiple resonant frequencies on bandwidth improvement. (b) Equivalent circuit transmission line model of a series-fed microstrip array.

$(i+1)$-th patch element due to the input impedance change by feed lines and the mutual coupling between adjacent patches. It introduces one additional resonant frequency in $Z_{\text{in},(i+1)}$. As a result, $Z_{\text{in},i}$ will have i-number of resonant frequencies. Furthermore, the feed lines have a uniform length of $l = 0.16\lambda_g$, which is much shorter than the conventional feed line length of $0.5\lambda_g$ where λ_g is a guided wavelength at the resonant frequency of the patch (26.5 GHz). By reducing l, the contribution of frequency change to the input impedance becomes smaller, implying that the input impedance variation among the neighboring resonant frequencies decreases. Thus, the multiple resonant frequencies are closely spaced, forming a broad impedance bandwidth. In a series-fed microstrip array, the real parts of $Z_{\text{in},i}$ at the resonant frequencies decrease as the number of array elements increases [24]. To minimize reflection at the edge of each feed line, the feed line widths are designed in a stepped manner ($w_1 \leq w_2 \leq, \ldots, \leq w_5$) with a gradual decrease in the characteristic impedance. Since the characteristic impedance is determined by the ratio of w_i to h, the rate of change of the feed line widths is defined as follows.

$$\alpha = \frac{w_{(i+1)} - w_i}{h} \tag{1}$$

Fig. 2(a) shows the efficacy of the proposed design approach on the impedance bandwidth of a series-fed array. When the small inter-element spacing ($l = 0.16\lambda_g$) is applied to the series-fed array, the number of resonant frequencies increases in proportion to the number of array elements from 1 to 5 and are closely spaced with each other. Note that these multiple resonant frequencies contribute not only to a broad bandwidth but also to flat gains over the wide frequency range. Furthermore, by adjusting the feed line widths in a stepped manner as $\alpha = 1$, the impedance matching at the edge of each feed line can be improved. As a result, a broader bandwidth is achieved as seen in the 5×1 array.

The input impedance $Z_{\text{in},i}$ and bandwidth of the proposed array can be formulated as follows. Fig. 2(b) presents the equivalent circuit transmission line model of a series-fed microstrip array. Each patch is represented by two parallel radiating slots with the admittance of Y_1 and Y_2 [25]. The admittance of slot 1 is given by $Y_1 = G_1 + jB_1$ where G_1 and B_1 are the conductance and susceptance of slot 1, respectively. Since the slot 2 is identical to slot 1, $G_1 = G_2$ and $B_1 = B_2$ (i.e., $Y_1 = Y_2$). The input admittance at the left edge of the 1st patch is denoted as $Y_{L,1}$, which is given by

$$\begin{aligned} Y_{L,1} &= Y_1 + \overline{Y_2} \\ &= Y_1 + Y_{0,A}\frac{Y_2 + jY_{0,A}\tan(\beta L_p)}{Y_{0,A} + jY_2\tan(\beta L_p)}, \end{aligned} \tag{2}$$

where $\beta = 2\pi/\lambda_g$, $Y_{0,A}$ is the characteristic admittance of a patch element, and $\overline{Y_2}$ is the transformed admittance of slot 2 from the right edge to the left edge of the patch. Since the two slots are separated by $L_p \simeq 0.5\lambda_g$, $\tan(\beta L_p) \simeq 0$ from 24 GHz to 30 GHz. Thus, $Y_{L,1} \simeq Y_1 + Y_2 = Y_A$ where Y_A represents the input admittance of a single patch. Then, the input admittance at the edge of the feed line connected to the 1st patch is given by

$$Y_{\text{in},1} = Y_{0,1}\frac{Y_{L,1} + jY_{0,1}\tan(\beta l)}{Y_{0,1} + jY_{L,1}\tan(\beta l)}, \tag{3}$$

where $Y_{0,1}$ is the characteristic admittance of the feed line. Herein, the tangent term in (3) can not be neglected because the proposed array has a small inter-element spacing of $l = 0.16\lambda_g$. Successively, $Y_{L,2} = Y_1 + \overline{Y_2 + Y_{\text{in},1}} \simeq Y_1 + Y_2 + Y_{\text{in},1} = Y_A + Y_{\text{in},1}$. Therefore, the input admittance $Y_{\text{in},i}$ can be generalized as

$$Y_{\text{in},i} = Y_{0,i}\frac{Y_{L,i} + jY_{0,i}\tan(\beta l)}{Y_{0,i} + jY_{L,i}\tan(\beta l)}, \tag{4}$$

where $Y_{0,i} = 1/Z_{0,i}$ is the characteristic admittance of the feed line connected to the i-th patch, and $Y_{L,i} = Y_A + Y_{\text{in},(i-1)}$ for $i = 1, 2, \ldots, N$ (N is a positive integer and $Y_{\text{in},0} = 0$). For a thin-metal mesh microstrip, the characteristic impedance $Z_{0,i}$ can be empirically found as follows [16].

$$Z_{0,i} = Z_{0,i}^{\text{solid}} + Z_{0,i}^{\text{correct}}, \tag{5}$$

$$Z_{0,i}^{\text{correct}} = \frac{0.46}{\sqrt{\varepsilon_{eff}^{\text{mesh}}}\rho^{1.35}}\left(\frac{h}{w_i}\right)^{0.75}, \frac{t}{\delta} < 3.3,$$

$$Z_{0,i}^{\text{correct}} = \frac{13}{\sqrt{\varepsilon_{eff}^{\text{mesh}}}\rho^{0.45}}\left(\frac{h}{w_i}\right)^{0.75}, \frac{t}{\delta} \geq 3.3, \tag{6}$$

where $Z_{0,i}^{\text{solid}}$ is the characteristic impedance of a conventional solid microstrip, $Z_{0,i}^{\text{correct}}$ is the correction term related to the filling factor ρ, $\varepsilon_{eff}^{\text{mesh}}$ is the effective dielectric constant of

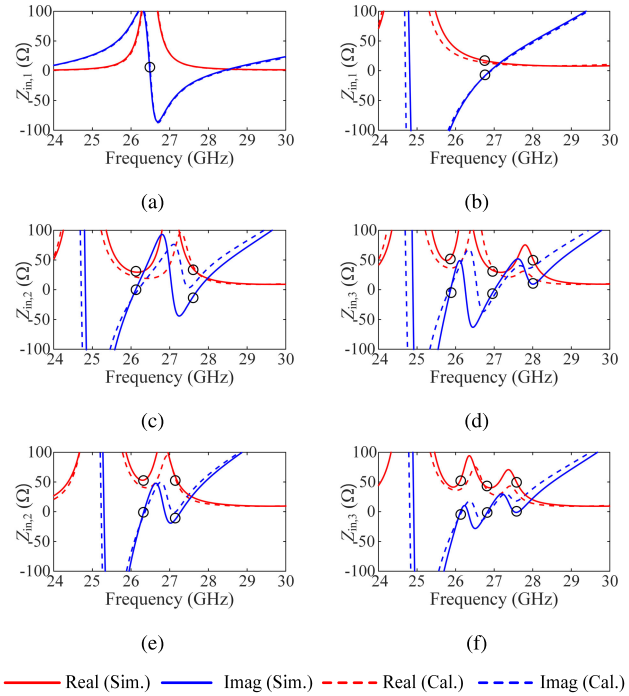

FIGURE 3. Simulated and calculated input impedance of the series-fed array. (a) $l = 0.5\lambda_g$ and $w_1 = 0.3$ mm. (b) $l = 0.16\lambda_g$ and $w_1 = 0.3$ mm. (c), (d) $l = 0.16\lambda_g$ and $\alpha = 0$ ($w_1 = 0.3$ mm). (e), (f) $l = 0.16\lambda_g$ and $\alpha = 1$ ($w_1 = 0.1$ mm). Resonant frequencies are marked by the black circle "O".

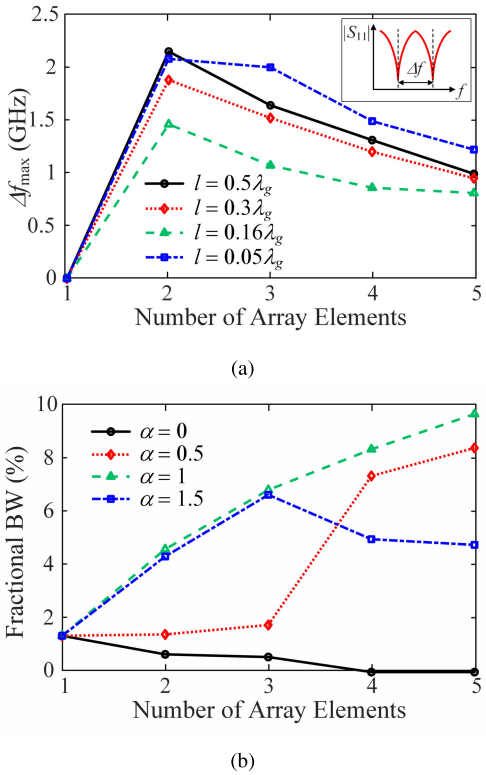

FIGURE 4. Parametric studies of l and α. Variation in (a) resonant frequency intervals according to l and (b) impedance bandwidth according to α as the number of array elements increases.

a thin-metal mesh microstrip, t is the width of the thin-metal line, and δ is the skin depth. Then, the input impedance can be obtained by $Z_{\text{in},i} = 1/Y_{\text{in},i}$, which is a function of frequency. The reflection coefficient at the edge of each feed line is defined as

$$\Gamma = \frac{Z_{\text{in},i} - Z_{0,i}}{Z_{\text{in},i} + Z_{0,i}}. \tag{7}$$

The -10 dB impedance bandwidth is defined as a frequency range satisfying $|\Gamma| \leq 0.32$.

Fig. 3 shows the simulated and calculated input impedance of the series-fed array. The calculated impedance shows good agreement with the simulated results. The resonant frequencies are marked by the black circle "O". In Fig. 3(a), when $l = 0.5\lambda_g$, the input impedance $Z_{\text{in},1}$ is almost identical to $Z_A = 1/Y_A$ with the same resonant frequency at 26.5 GHz. In contrast, the overall input impedance is shifted toward the lower frequencies when $l = 0.16\lambda_g$ as Fig. 3(b). Since $Y_{L,(i+1)} = Y_A + Y_{\text{in},i}$, this introduces an additional resonant frequency where the imaginary part of $Y_{L,(i+1)}$ becomes 0. From Fig. 3(b) to 3(d), it can be seen that one additional resonance is introduced at a higher frequency as the number of array elements increases from i to $i + 1$. In addition, the existing resonant frequencies in $Z_{\text{in},i}$ are shifted toward lower frequencies in $Z_{\text{in},(i+1)}$ and closely spaced from each other. However, the input impedance still has a large variation in both real and imaginary parts between the resonant points. When the stepped feed lines with $\alpha = 1$ are applied, the impedance variation between the resonant points is reduced as Figs. 3(e) and 3(f). Also, the intervals between resonant points are more closely spaced compared to those in Figs. 3(c) and 3(d), which allows for improvement in impedance bandwidth.

III. INVESTIGATION OF DESIGN PARAMETERS

To demonstrate the effectiveness of the proposed design approach, the antenna characteristics are analyzed by using full-wave numerical simulation, Ansys HFSS. Considering the enormous computational time required for the thin-metal mesh structure, the series-fed array is simulated as a solid metal structure. Fig. 4(a) presents the variation in resonant frequency intervals for l. In the simulation, all the feed line widths are fixed as 0.3 mm with 50-Ω characteristic impedance. As presented in the upper right corner of the figure, Δf denotes the resonant frequency interval within the frequency range of 24−30 GHz. $\Delta f_{\max}$ indicates maximum among the multiple resonant frequency intervals. Overall, $\Delta f_{\max}$ is reduced as the number of array elements increases. When the number of array elements is more than 1, $\Delta f_{\max}$ gradually decreases as l decreases from $0.5\lambda_g$ to $0.16\lambda_g$, which implies that the multiple resonant frequencies are positioned closely enough to form a broad bandwidth. On the other hand, when l is too small such as $0.05\lambda_g$, $\Delta f_{\max}$ significantly increases. This drastic change in resonant frequency intervals is mainly due to the strong mutual

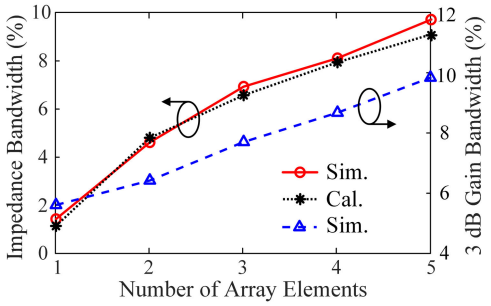

FIGURE 5. Simulated impedance and 3 dB gain bandwidths of the series-fed array with respect to the number of array elements.

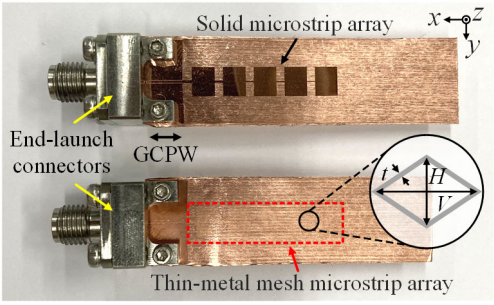

FIGURE 6. Fabricated series-fed microstrip array antennas; solid microstrip array (top) and thin-metal mesh microstrip array (bottom).

coupling effect between adjacent patch elements. Fig. 4(b) shows the variation in −10 dB impedance bandwidth with respect to α. When $\alpha = 0$, the bandwidth decreases as the number of array elements increases because of impedance mismatch. As α increases from 0 to 1, the bandwidth improves in all array designs due to the better impedance matching at the edge of each feed line. However, when α increases to 1.5, the bandwidth degrades compared to the case of $\alpha = 1$. This is because the large α leads to a very low characteristic impedance of the feed line, causing an impedance mismatch with the input impedance. Hence, for better impedance matching, the value of α needs to be adjusted at each feed line.

Fig. 5 presents the enhancement of impedance and 3 dB gain bandwidths of the series-fed array as the number of array elements increases. The array is optimized with $l = 1.3$ mm, $w_1 = 0.1$ mm, $w_2 = 0.2$ mm, $w_3 = 0.2$ mm, $w_4 = 0.4$ mm, and $w_5 = 0.42$ mm. By the proposed design approach, the −10 dB impedance bandwidth improves from 1.3% for the single microstrip antenna to 9.7% for the 5 × 1 array. Besides, the 3 dB gain bandwidth is also increased from 5.6% for the single microstrip antenna to 9.8% for the 5 × 1 array. The calculated impedance bandwidth from (7) is well-matched to the simulated result. In the calculation, the mutual coupling effects and loss in the microstrip are not included. The simulated peak gains are 6.4 dBi for the single antenna and 11.6 dBi for the 5 × 1 array. It is shown that the impedance and gain bandwidths of the proposed antenna can be further improved by increasing the number of array elements.

TABLE 1. Design parameters of the solid microstrip array.

i	W_p (mm)	L_p (mm)	l (mm)	w_i (mm)	$Z_{0,i}$ (Ω)
1	4.60	3.58	1.30	0.10	96.5
2	4.60	3.58	1.30	0.20	65.9
3	4.60	3.58	1.30	0.20	65.9
4	4.60	3.58	1.30	0.40	41.6
5	4.60	3.58	1.30	0.42	40.1

TABLE 2. Design parameters of the thin-metal mesh microstrip array.

i	W_p (mm)	L_p (mm)	l (mm)	w_i (mm)	$Z_{0,i}$ (Ω)
1	4.62	3.58	1.32	0.12	106.1
2	4.62	3.58	1.32	0.24	67.8
3	4.62	3.58	1.32	0.24	67.8
4	4.62	3.58	1.32	0.54	41.7
5	4.62	3.58	1.32	0.54	41.7

IV. FABRICATION AND MEASUREMENT

A. IMPEDANCE BANDWIDTH AND RADIATION PATTERN

Fig. 6 shows the fabricated series-fed microstrip array antennas. Both solid and thin-metal mesh microstrip arrays are fabricated to compare their performance with each other. The feed lines and patch elements are patterned on a transparent COP film ($\varepsilon_r = 2.32$, $\tan\delta = 0.0006$) with $h = 100$ μm using a photolithography process. The optically transparent microstrip array consists of unit meshes. The unit mesh with dimensions of $H \times V = 60$ μm × 120 μm is designed to surround the RGBG diamond-shaped PenTile LEDs [26] in the display of a commercial smartphone (Samsung Galaxy S10+). The thin-metal lines of the meshes are placed within the micro-scale gap between adjacent LEDs. To maximize the optical transparency while avoiding significant ohmic losses from the skin depth of $\delta = 0.39$ μm, the thin-metal line made of copper has a width of $t = 1$ μm and a thickness of 1 μm. The optimized design parameters for the solid and thin-metal mesh microstrip array are listed in Table 1 and Table 2, respectively. The thin-metal mesh microstrip line has discretized characteristic impedance due to the discretized dimension of the unit mesh. Moreover, it features a higher impedance for the same w_i compared to the solid microstrip, which results in a large variation in the input impedance. For these reasons, w_i of both solid and thin-metal mesh array is optimized based on the discretized $Z_{0,i}$ of the thin-metal mesh microstrip in [16]. As a result, the feed line widths are designed in a stepped manner ($w_1 \leq w_2$, …, $\leq w_5$) but not in a strictly increasing manner ($w_1 < w_2$, …, $< w_5$). In addition, the feed line widths of the thin-metal mesh microstrip are designed to be larger than those of the solid microstrip for the same impedance $Z_{0,i}$. Underneath the dielectric substrate, a 60 μm-thick copper GND is located. A 50-Ω GCPW is adopted for the interface with the end-launch connector. The optical transparency of the fabricated thin-metal mesh microstrip array is measured using a haze meter (Nippon Denshoku NDH-2000). It exhibits an average transparency of 85.1% in the visible light wavelength range of 400 nm to 700 nm.

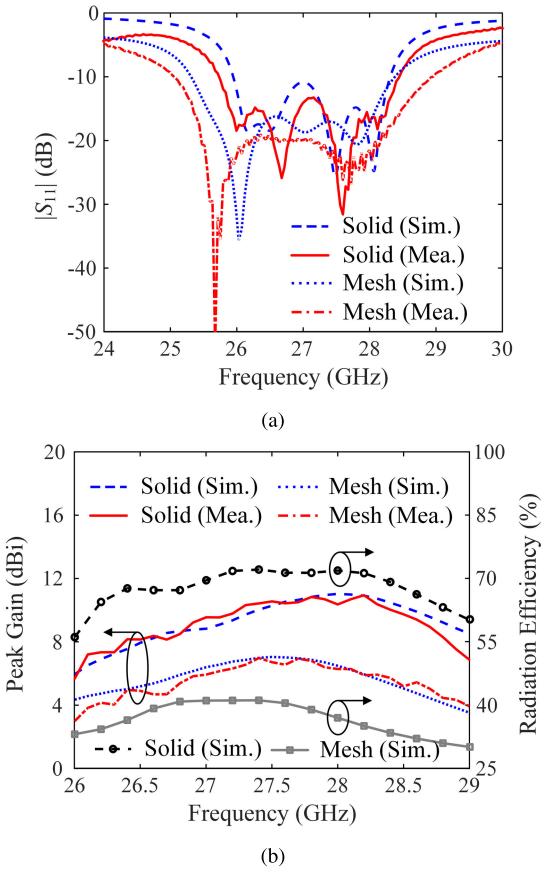

FIGURE 7. Simulated and measured results of the proposed array antennas. (a) Reflection coefficients. (b) Peak gains and radiation efficiencies.

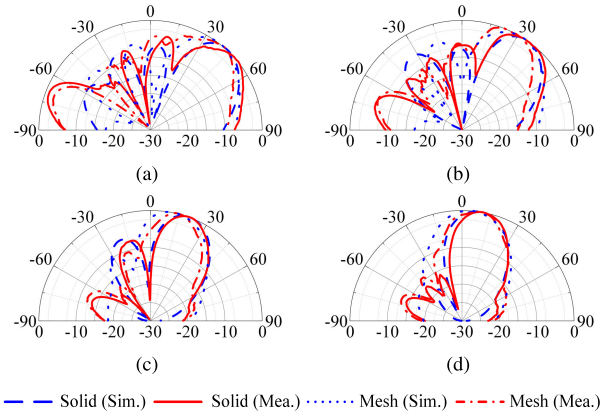

FIGURE 8. Normalized E-plane radiation patterns of the proposed array antennas at (a) 26 GHz, (b) 26.5 GHz, (c) 27.4 GHz, and (d) 28.1 GHz.

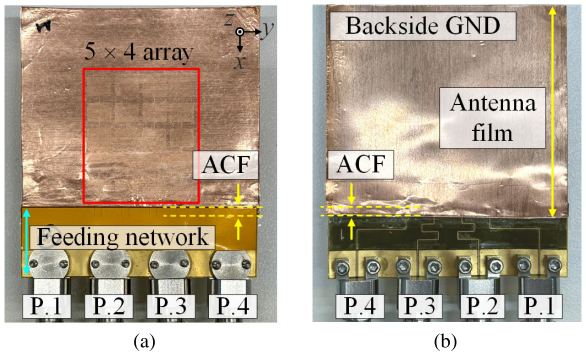

FIGURE 9. Fabricated 5 × 4 array antenna with the feeding network. (a) Top view. (b) Bottom view.

Figs. 7(a) and 7(b) display the reflection coefficient and peak gain of the proposed series-fed array antennas. The reflection coefficients and radiation patterns of the fabricated antennas are measured in a full anechoic chamber using a vector network analyzer (VNA). The simulated impedance bandwidth of the solid microstrip array is 2.36 GHz (25.95−28.31 GHz), while the measured bandwidth is 2.72 GHz (25.72−28.44 GHz) showing good agreement with the simulated result. The fabricated solid array exhibits a peak gain of above 5.71 dBi from 26 GHz to 29 GHz with a maximum value of 11 dBi at 28.2 GHz. The measured bandwidth of the thin-metal mesh array is 3.84 GHz (25.08−28.92 GHz) while the simulated bandwidth is 3.08 GHz (25.32−28.4 GHz), which is much broader than that of the solid array. Within the overall frequency range, the thin-metal mesh array achieves a peak gain of above 3.05 dBi with a maximum value of 7.02 dBi at 27.4 GHz. Also, the array shows a broad 3 dB gain bandwidth of 2.8 GHz (26.2−29 GHz). The broader bandwidth of the thin-metal mesh array is attributed to the higher sheet resistance (0.12 Ω/sq) than that of the solid array (0.02 Ω/sq), which also affects the gain degradation. As shown in Fig. 7(b), the thin-metal mesh array exhibits lower average radiation efficiency (37%) from 26 GHz to 29 GHz compared to the solid array (68%). Compared to conventional microstrip arrays with an inter-element spacing of $l = 0.5\lambda_g$, the proposed array with $l = 0.16\lambda_g$ features a peak gain drop of about 1.3 dB. It is attributed to the mutual coupling between the closely spaced array elements, affecting the excitation phase of the patches as well. From the measured results, it is confirmed that the proposed design approach is effective for achieving both impedance bandwidth and flat gains over the wide frequency range.

Fig. 8 shows the normalized E-plane (*xz*-cut) radiation pattern of the proposed antennas. The measured radiation patterns of the solid array are in good agreement with the simulation results. The thin-metal mesh array also shows similar radiation patterns. As frequency increases from 26 GHz to 28.1 GHz, the peak gain direction of the thin-metal mesh array varies from 44° to 11° (close to the broadside direction), and the side lobes gradually decrease. This beam steering characteristic is due to a phase shift between the adjacent patch elements. Since the phase shift decreases as frequency increases, the peak gain direction is shifted towards the broadside.

B. BEAM SCANNING PROPERTIES

To evaluate the beam scanning performance of the proposed array for mobile wireless communications, a 5 × 4 array

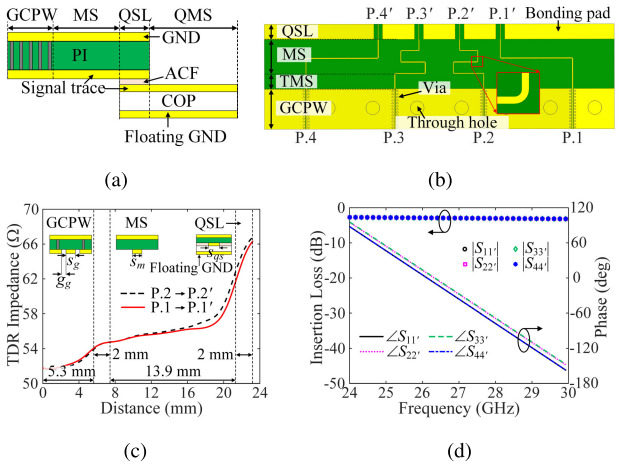

FIGURE 10. Design of the feeding network and simulated results. (a) Side view. (b) Top view. (c) TDR impedance. (d) Transmission losses and phases.

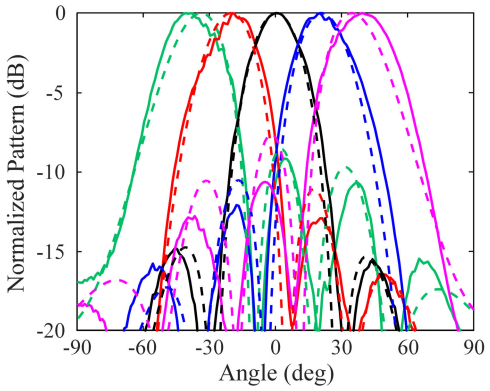

FIGURE 11. Synthesized H-plane beam patterns of the phased array at 28 GHz; solid lines are measured patterns and dashed lines are simulated patterns.

antenna is fabricated as shown in Fig. 9. The array spacing in y-direction is 5.35 mm which is half-wavelength at 28 GHz. From left to right, each 5 × 1 array is connected to the individual port through the feeding network. The feeding network printed on a PI substrate ($\varepsilon_r = 2.45$, $\tan\delta = 0.02$) with a thickness of 50 μm has four transmission lines with a uniform length of 23.2 mm for in-phase excitation.

As Figs. 10(a) and 10(b), the feeding network consists of three different transmission line sections: GCPW; microstrip (MS) with tapered trace width; and quasi-stripline (QSL). The signal traces of PI substrate and COP are bonded to each other using ACF. It should be noted that the GND on the bottom of COP is not electrically connected to the GND of the PI substrate (i.e., floating GND) since implementing via posts is prohibited by the manufacturing process of display panels. Thus, the transmission line in the bonding section has QSL mode, and the antenna operates in quasi-microstrip (QMS) mode. Since the width of the end-launch connector (11.68 mm) is much larger than the array spacing, the feeding network has a fan-out shape and symmetry to the x-axis. The feeding network design is optimized by following Step 1−3 in Fig. 10(c) for gradual time domain reflectometry (TDR) impedance transitions: In Step 1, the GCPW structure is designed for connection with an end-launch connector. It has a signal trace width of $s_g = 0.12$ mm and a gap of $g_g = 0.06$ mm between the signal trace and the coplanar GND to achieve a 50-Ω impedance. The via posts are designed with a diameter of 0.2 mm and an edge-to-edge distance of 0.2 mm to prevent wave leakage. In Step 2, the MS line width (s_m) is tapered (TMS) from 0.12 mm to 0.115 mm within a length of 2 mm for impedance matching with the GCPW. Then, the MS line from Port 2 to Port 2′ (Port 3 to Port 3′) is meandered to have an equal line length from Port 1 to Port 1′ (Port 4 to Port 4′). Rounded edges are applied at each 90° bend of the line to minimize reflection losses as depicted in Fig. 10(b). In Step 3, the MS is transformed to the QSL with the impedance change from 50 Ω to 60 Ω by varying s_{qs} from 0.12 mm to 0.07 mm. To maintain QSL mode, the bonding pads have an edge-to-edge distance of 0.55 mm from the signal trace. In Fig. 10(d), the feeding network shows the simulated insertion loss of 2.5 dB including dielectric, conduction, and return losses, with a phase difference of 8.2° between the two different pairs of ports. The gradual increase in the TDR impedance within each section is mainly from dielectric and conduction losses. The active element pattern (AEP) is measured at each port while terminating the other ports with 50-Ω loads [27]. Then, the measured AEPs are synthesized to produce the array beam pattern.

Fig. 11 presents the synthesized H-plane (yz-cut) beam pattern of the phased array. The fabricated 5 × 4 array with no phase shift exhibits 11.8 dBi bore-sight gain. When progressive phase shifts of ±70° and ±120° are applied, the beam is steered to $\theta = \mp 20°$ and $\mp 40°$ with a gradual increase in the sidelobe level up to −9.2 dB and scan loss up to 3.6 dB. Note that the measured loss in the ACF bonding section is 0.3 dB, which is included in the 2.3 dB total loss of the feeding network. Since the insertion loss lowers the gain of each AEP, it is compensated before synthesizing the beam pattern.

The result of this work is compared with previous works for antenna-on-display applications in Table 3. Compared to [12], [14], [16], [18], the proposed antenna shows a broad bandwidth with a lower profile in terms of wavelength. In addition, the proposed design exhibits a much higher single antenna gain than other works while showing optical transparency of above 80%. The proposed series-fed microstrip array has a much broader impedance bandwidth and higher gain compared to our previous work in [16]. The impedance bandwidth and flat gain of a series-fed microstrip array can be further improved by increasing the number of array elements using the proposed design approach. Moreover, beam scanning properties of the antenna up to ±40° are demonstrated through the 1 × 4 feeding network for use in mobile wireless communications, which is not covered in [16]. Note that the array is fabricated as a proof-of-concept of the proposed approach and optical invisibility is not considered in this work. To enable optical invisibility [14], [15] for practical AoD applications, our antenna design

TABLE 3. Comparison with previous works for antenna-on-display applications.

Reference	Frequency (GHz)	Impedance bandwidth (%)	Maximum gain of single antenna (dBi)	3 dB gain bandwidth (%)	Metallic material	Transparency (%)	Antenna profile (λ_0)	Scanning angle (°)
[12]	26	22	2.0	22.9	ITO film	84	0.0935	N/A.
[14]	28	6.4	4.05	N/A.	Ag-alloy	**88	0.0784	±60
[15]	2.4	22.2	1.73	N/A.	Cu	**97	0.0004	N/A.
[16]	28	3.32	1.7	8.84	Cu	96	0.0093	N/A.
[17]	2.45	N/A.	4.14	N/A.	Cu	82.6	0.0098	N/A.
[18]	28	17.8	*1.9	N/A.	Ag-alloy	N/A.	0.0210	±40
This work	27	14.2	7.02	10.1	Cu	85.1	0.0093	±40

*It includes losses by interconnection and feeding networks.
**Optical invisibility is considered in antenna design.
The antenna profile of [12], [14], [15], [16], [17], and this work does not include the substrate thickness for feeding network.

can employ dummy-grid patterns, which are identical to the unit mesh and spaced with small intervals from the antenna patterns. Moreover, black oxide coating can be utilized after the photolithography process to minimize light reflection [28].

V. CONCLUSION

This paper proposed an optically transparent series-fed microstrip array with small inter-element spacing and stepped feed lines for AoD application. By using small inter-element spacing and stepped feed lines, both impedance bandwidth and flat gain are enhanced as the number of array elements increases. The proposed design approach and its effectiveness were demonstrated by the simulated results. Then, 5 × 1 and 5 × 4 series-fed arrays were fabricated and measured. In measurement, the fabricated 5 × 1 array showed a −10 dB impedance bandwidth of 3.84 GHz (25.08−28.92 GHz) and a 3 dB gain bandwidth of 2.8 GHz (26.2−29 GHz) with a peak gain of 7.02 dBi at 27.4 GHz. Moreover, the beam scanning performance for the 5 × 4 array was evaluated, showing ±20° and ±40° at 28 GHz with a bore-sight gain of 11.8 dBi.

REFERENCES

[1] W. Hong, Z. H. Jiang, C. Yu, D. Hou, H. Wang, C. Guo, Y. Hu, L. Kuai, Y. Yu, Z. Jiang, Z. Chen, J. Chen, Z. Yu, J. Zhai, N. Zhang, L. Tian, F. Wu, G. Yang, Z.-C. Hao, and J. Y. Zhou, "The role of millimeter-wave technologies in 5G/6G wireless communications," *IEEE J. Microw.*, vol. 1, no. 1, pp. 101–122, Jan. 2021.

[2] W. Han, F. Yang, J. Ouyang, and P. Yang, "Low-cost wideband and high-gain slotted cavity antenna using high-order modes for millimeter-wave application," *IEEE Trans. Antennas Propag.*, vol. 63, no. 11, pp. 4624–4631, Nov. 2015.

[3] B. G. P. Shariff, T. Ali, P. R. Mane, and P. Kumar, "Array antennas for mmWave applications: A comprehensive review," *IEEE Access*, vol. 10, pp. 126728–126766, 2022.

[4] M. Marcus and B. Pattan, "Millimeter wave propagation: Spectrum management implications," *IEEE Microw. Mag.*, vol. 6, no. 2, pp. 54–62, Jun. 2005.

[5] H. Chen, Y. Shao, Y. Zhang, C. Zhang, and Z. Zhang, "A low-profile broadband circularly polarized mmWave antenna with special-shaped ring slot," *IEEE Antennas Wireless Propag. Lett.*, vol. 18, pp. 1492–1496, 2019.

[6] J. Kim and H. L. Lee, "High gain planar segmented antenna for mmWave phased array applications," *IEEE Trans. Antennas Propag.*, vol. 70, no. 7, pp. 5918–5922, Jul. 2022.

[7] B. Yu, K. Yang, C.-Y.-D. Sim, and G. Yang, "A novel 28 GHz beam steering array for 5G mobile device with metallic casing application," *IEEE Trans. Antennas Propag.*, vol. 66, no. 1, pp. 462–466, Jan. 2018.

[8] D. V. Navarro-Méndez, L. F. Carrera-Suárez, E. Antonino-Daviu, M. Ferrando-Bataller, M. Baquero-Escudero, M. Gallo, and D. Zamberlan, "Compact wideband Vivaldi monopole for LTE mobile communications," *IEEE Antennas Wireless Propag. Lett.*, vol. 14, pp. 1068–1071, 2015.

[9] T. D. Nguyen, K. Kim, S. R. Yoon, and G. Byun, "Optically invisible artificial magnetic conductor subarrays for triband display-integrated antennas," *IEEE Trans. Microw. Theory Techn.*, vol. 70, no. 8, pp. 3975–3986, Aug. 2022.

[10] C.-L. Lin, F.-H. Chen, W.-C. Ciou, Y.-W. Du, C.-E. Wu, and C.-E. Lee, "Simplified gate driver circuit for high-resolution and narrow-bezel thin-film transistor liquid crystal display applications," *IEEE Electron Device Lett.*, vol. 36, no. 8, pp. 808–810, Aug. 2015.

[11] K. Fujita and M. Takahashi, "A concept of transparent antenna array on touch screen panel for sub-6 GHz cellular devices," in *Proc. IEEE Int. Symp. Antennas Propag. USNC-URSI Radio Sci. Meeting (APS/URSI)*, Dec. 2021, pp. 3–4.

[12] K. K. So, B.-J. Chen, and C. H. Chan, "Microwave and millimeter-wave MIMO antenna using conductive ITO film," *IEEE Access*, vol. 8, pp. 207024–207033, 2020.

[13] Q. L. Li, S. W. Cheung, D. Wu, and T. I. Yuk, "Optically transparent dual-band MIMO antenna using micro-metal mesh conductive film for WLAN system," *IEEE Antennas Wireless Propag. Lett.*, vol. 16, pp. 920–923, 2017.

[14] J. Park, S. Y. Lee, J. Kim, D. Park, W. Choi, and W. Hong, "An optically invisible antenna-on-display concept for millimeter-wave 5G cellular devices," *IEEE Trans. Antennas Propag.*, vol. 67, no. 5, pp. 2942–2952, May 2019.

[15] W. Hong, S. Lim, S. Ko, and Y. G. Kim, "Optically invisible antenna integrated within an OLED touch display panel for IoT applications," *IEEE Trans. Antennas Propag.*, vol. 65, no. 7, pp. 3750–3755, Jul. 2017.

[16] J. M. Heo, E. J. Sung, J. K. Kim, and G. Byun, "Characteristic impedance adjustment of thin-metal mesh transmission lines for mmWave display-integrated antennas," *IEEE Access*, vol. 9, pp. 94714–94722, 2021.

[17] S. H. Kang and C. W. Jung, "Transparent patch antenna using metal mesh," *IEEE Trans. Antennas Propag.*, vol. 66, no. 4, pp. 2095–2100, Apr. 2018.

[18] D. Lee, B. Kim, J. Lee, Y. Youn, M. Kim, S. Chang, D. Park, and W. Hong, "Dual-polarized dual-band antenna-on-display using via-less and single-layer topology for mmWave wireless scenarios," *IEEE Antennas Wireless Propag. Lett.*, vol. 22, pp. 1000–1004, 2023.

[19] M. Khalily, R. Tafazolli, P. Xiao, and A. A. Kishk, "Broadband mm-wave microstrip array antenna with improved radiation characteristics for different 5G applications," *IEEE Trans. Antennas Propag.*, vol. 66, no. 9, pp. 4641–4647, Sep. 2018.

[20] W. C. Yang, H. Wang, W. Q. Che, Y. Huang, and J. Wang, "High-gain and low-loss millimeter-wave LTCC antenna array using artificial magnetic conductor structure," *IEEE Trans. Antennas Propag.*, vol. 63, no. 1, pp. 390–395, Jan. 2015.

[21] T. Yuan, N. Yuan, and L.-W. Li, "A novel series-fed taper antenna array design," *IEEE Antennas Wireless Propag. Lett.*, vol. 7, pp. 362–365, 2008.

[22] R. Chopra and G. Kumar, "Series-fed binomial microstrip arrays for extremely low sidelobe level," *IEEE Trans. Antennas Propag.*, vol. 67, no. 6, pp. 4275–4279, Jun. 2019.

[23] H. Yi, L. Li, J. Han, and Y. Shi, "Traveling-wave series-fed patch array antenna using novel reflection-canceling elements for flexible beam," *IEEE Access*, vol. 7, pp. 111466–111476, 2019.

[24] A. Muduli and R. K. Mishra, "Transmission line model for a series fed log-periodic microstrip antenna array," in *Proc. 14th IEEE India Council Int. Conf. (INDICON)*, Dec. 2017, pp. 1–3.
[25] C. A. Balanis, *Antenna Theory: Analysis and Design*. Hoboken, NJ, USA: Wiley, 2016, pp. 793–794.
[26] J.-H. Lee, K.-R. Kim, and C.-S. Kim, "Subpixel rendering without color distortions for diamond-shaped PenTile displays," in *Proc. IEEE Int. Symp. Circuits Syst. (ISCAS)*, May 2017, pp. 1–4.
[27] D. M. Pozar, "The active element pattern," *IEEE Trans. Antennas Propag.*, vol. 42, no. 8, pp. 1176–1178, Aug. 1994.
[28] E. Oberg, F. D. Jones, H. L. Horton, and H. H. Ryffel, *Machinery's Handbook: A Reference Book for the Mechanical Engineer, Designer, Manufacturing Engineer, Draftsman, Toolmaker, and Machinist*, 24th ed. New York, NY, USA: Industrial Press, 1992, p. 1444.

JIN MYEONG HEO (Graduate Student Member, IEEE) received the B.S. degree in electrical and computer engineering from Ulsan National Institute of Science and Technology (UNIST), Ulsan, South Korea, in 2019, where he is currently pursuing the combined M.S./Ph.D. degree in electrical engineering. His research interests include display-integrated antennas, optically transparent antennas/transmission lines, and beamforming array antennas.

KISEO KIM received the M.S. degree in physics from Kyung-Hee University, Seoul, South Korea, in 2008. He is currently an Engineer with Samsung Display. His research interests include display integrated antenna and next-generation displays.

JAEUK CHOI received the bachelor's degree in physics from the Kumoh National Institute of Technology, in 2014. He is currently an Engineer with Samsung Display. His research interest includes RF-antenna available on display.

GANGIL BYUN (Senior Member, IEEE) received the B.S. and M.S. degrees in electronic and electrical engineering from Hongik University, Seoul, South Korea, in 2010 and 2012, respectively, and the Ph.D. degree in electronics and computer engineering from Hanyang University, Seoul, in 2015.

Following his graduation, he joined Hongik University as a Research Professor, where he conducted active research for two years. In February 2018, he joined as a Faculty Member of Ulsan National Institute of Science and Technology (UNIST), Ulsan, South Korea, where he is currently an Associate Professor with the Department of Electrical Engineering (EE). Since 2022, he has been the Director of the Core RF/Power Component Research Center for Low-Orbit Next-Generation Satellites (LONGS). His primary research focuses on millimeter-wave antennas and metasurfaces, with a strong emphasis on advancing adaptive beamforming techniques for diverse applications, including 5G/6G communication, satellite technology, defense systems, and radars. His distinguished contributions have been pivotal in advancing overall beamforming performance, achieved through a unique integration of antenna engineering, and signal processing insights. His current research pursuits extend to display-integrated antennas, antenna-in-package (AiP), and reconfigurable intelligent surface (RIS) to derive innovations for future wireless communication systems.